NANO LETTERS

pubs.acs.org/NanoLett Letter

Engineering Directionality in Quantum Dot Shell Lasing Using Plasmonic Lattices

Jun Guan, Laxmi Kishore Sagar, Ran Li, Danqing Wang, Golam Bappi, Nicolas E. Watkins, Marc R. Bourgeois, Larissa Levina, Fengjia Fan, Sjoerd Hoogland, Oleksandr Voznyy, Joao Martins de Pina, Richard D. Schaller, George C. Schatz, Edward H. Sargent, and Teri W. Odom*

Cite This: *Nano Lett.* 2020, 20, 1468−1474 Read Online

ACCESS | Metrics & More | Article Recommendations | Supporting Information

ABSTRACT: We report how the direction of quantum dot (QD) lasing can be engineered by exploiting high-symmetry points in plasmonic nanoparticle (NP) lattices. The nanolaser architecture consists of CdSe−CdS core−shell QD layers conformally coated on two-dimensional square arrays of Ag NPs. Using waveguide-surface lattice resonances (W-SLRs) near the Δ point in the Brillouin zone as optical feedback, we achieved lasing from the gain in CdS shells at off-normal emission angles. Changing the periodicity of the plasmonic lattices enables other high-symmetry points (Γ or M) of the lattice to overlap with the QD shell emission, which facilitates tuning of the lasing direction. We also increased the thickness of the QD layer to introduce higher-order W-SLR modes with additional avoided crossings in the band structure, which expands the selection of cavity modes for any desired lasing emission angle.

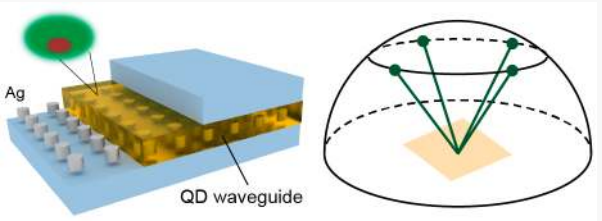

KEYWORDS: *lattice plasmons, surface lattice resonances, waveguide, band structure engineering, colloidal quantum dots, laser directionality*

Colloidal quantum dots (QDs) are attractive gain materials for coherent light sources.[1,2] Unlike epitaxial semiconductors that require complex deposition steps, these nanocrystals can be solution-processed,[3] and compared to dye molecules, they exhibit high photoluminescence quantum yields[4] and long-term photostability.[5] Stimulated emission from QDs has previously been a challenge due to nonradiative Auger losses,[6,7] where electron−hole recombination energy is transferred to a third charge carrier instead of being emitted as a photon. To suppress Auger rates, core−shell geometries are widely used because a shell consisting of a wider-bandgap material enables spatial separation of the electrons and holes across the QD with weakened carrier coupling.[2,7] Besides enhancing the optical gain of the core material, large shell volumes (>10 monolayers) can also show stimulated emission.[8−10] Lasing has been demonstrated from both QD cores and shells using different cavity architectures,[1] including ring structures,[8] dielectric microspheres,[11,12] photonic crystals,[13,14] and plasmonic block reflectors;[15] however, tuning of the direction of QD lasing is lacking.

Engineering the direction of lasing beams is important for laser projection displays,[16] remote sensing,[17] and on-chip optical interconnects.[18,19] Diffractively coupled plasmonic nanoparticle (NP) arrays support surface lattice resonances (SLRs)[20,21] whose photonic band structure can be manipulated by various design parameters including the refractive index environment,[22] lattice geometry,[23−25] and NP size.[26−28] When combined with gain media, plasmonic lattices can provide optical feedback for lasing with directional emission.[29−33] Although lasing emission at off-normal angles has been shown in NP superlattices,[34] finite lattices,[35] and honeycomb lattices,[36] the available tuning range is small ($\Delta\theta < 3°$) in these designs because of limited access to band-edge modes. Expanding the types of plasmonic modes available for optical feedback is necessary for wide-range control of lasing directionality. Since a closely packed QD layer can function as an optical waveguide,[6] integrating QDs with plasmonic lattices may provide a route to design cavity modes through both array symmetry and waveguide architectures.

Here we show how QD lasing directionality can be engineered by exploiting high-symmetry points in plasmonic NP square lattices. We built QD nanolasers by conformally coating CdSe−CdS core−shell QDs on a 2D Ag NP array. Near the Δ point of the square lattice, hybrid waveguide-surface lattice resonance (W-SLR) modes facilitate lasing emission at off-normal angles. The lasing beams are

Received: December 30, 2019
Revised: January 25, 2020
Published: January 31, 2020

https://dx.doi.org/10.1021/acs.nanolett.9b05342
Nano Lett. 2020, 20, 1468−1474

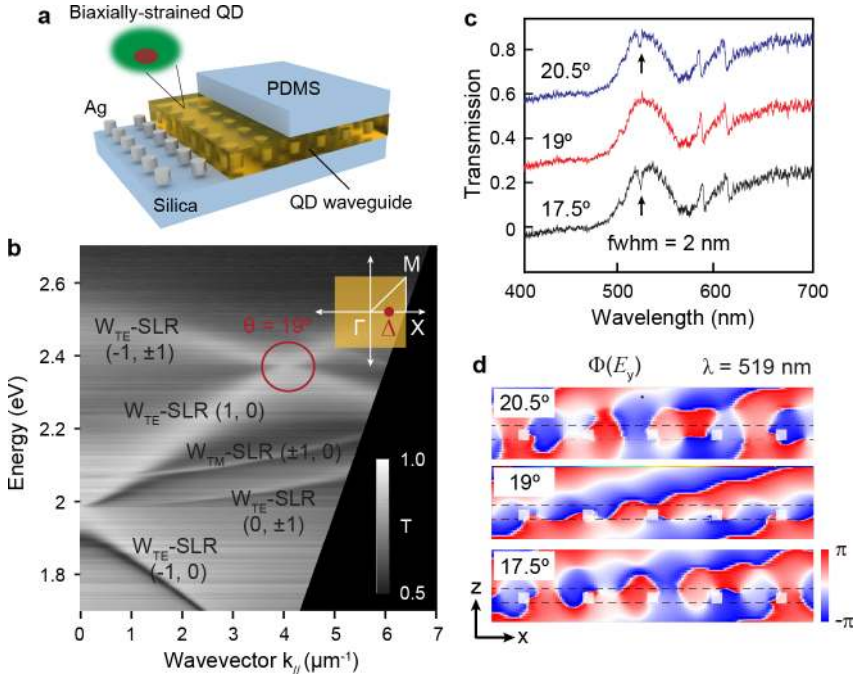

Figure 1. Design of W-SLR sidebands near the Δ point. (a) Scheme of plasmonic lattices integrated with the QD waveguide. The lattice spacing is 400 nm. Ag cylindrical NPs are of 70 nm diameter and 60 nm height. The QD film is ∼90 nm thick. (b) Measured band structure of the QD-plasmon device under s-polarized incident light along the Γ−X direction. The inset shows the reciprocal space Brillouin zone and the high-symmetry points Γ, X, M, and Δ. The red circle indicates the Δ point on the band structure. (c) Measured transmission spectra under s-polarized incident light with excitation angles of 20.5, 19, and 17.5° near the Δ point. Transmission spectra at 19 and 17.5° were shifted down 0.3 and 0.6, respectively, for clarity. (d) Simulated phase maps at 519 nm with excitation angles of 20.5, 19, and 17.5°.

azimuthally polarized with a donut shape because of the optical feedback from the sidebands of the W-SLR modes. By varying the periodicity of the plasmonic lattices, we tuned other high-symmetry points (Γ or M) to overlap with the CdS shell emission to control different lasing angles. Finally, we increased the thickness of the QD film to access higher-order W-SLR modes with avoided crossings in the photonic band structure, thereby expanding the selection of cavity modes to realize any desired lasing emission angle.

Figure 1a depicts a laser architecture consisting of a CdSe−CdS QD waveguide layer on a Ag NP lattice. First, we fabricated 2D square arrays of Ag NPs (spacing a_0 = 400 nm, diameter d = 70 nm, height h = 60 nm) on fused silica using solvent-assisted nanoscale embossing (SANE[37]) and PEEL processes.[38,39] Second, we synthesized biaxially strained, core−shell QDs[40] with ∼3.2 nm diameter cores and ∼15.7 nm diameter shells (Figures S1 and S2) that we spin-cast on the NP lattices into a densely packed film. The large volume of the CdS shells compared to the CdSe cores resulted in strong shell photoemission at ∼520 nm under high pump powers (Figure S3). Next, we placed a slab of poly(dimethylsiloxane) (PDMS, n ∼ 1.43) on top of the QD film as a protective layer to ensure mechanical robustness of the QD film surface. The high refractive index of the QD film (n ∼ 1.95 at 520 nm) (Figure S3) and high film thickness (90 nm) (Figure S4) ensured that the QD layer functioned as an optical waveguide. Coupling of waveguide modes in the QD layer and SLRs in the Ag NP lattice produced W-SLR modes (Figure 1b and Figure S5). The hybrid modes are indexed as $W_{TE/TM}$-SLR(m_1, m_2), where $W_{TE/TM}$ refers to transverse electric (TE) or transverse magnetic (TM) mode of the zero-order waveguide mode and (m_1, m_2) indicates the Bragg diffraction orders of the lattice. The reciprocal vector $\mathbf{G}$ is given by $\mathbf{G} = m_1\mathbf{b_1} + m_2\mathbf{b_2}$, where $\mathbf{b_1}$ and $\mathbf{b_2}$ are the primitive vectors of the reciprocal lattice. In the Brillouin zone, the high-symmetry point Δ is defined as the middle point between the Γ and X points with $\mathbf{k}_{||} = \frac{1}{4}\mathbf{b_1}$ (Figure 1b, Figure S5). Based on the empty-lattice dispersion relation $|\mathbf{k}_{||} + \mathbf{G}| = n_{\text{eff}}\frac{\omega}{c}$, three diffraction modes (−1, 1), (−1, −1), and (1, 0) are degenerate in energy at the Δ point. We designed the plasmonic NP lattice and QD film thickness using finite-difference time-domain (FDTD) simulations to overlap this Δ point energy with the CdS QD shell emission (500−530 nm) (Figure S5). Near the Δ point (E = 2.4 eV, $|\mathbf{k}_{||}|$ = 4 μm^{-1}), W_{TE}-SLR modes are produced at excitation angles of 17.5 and 20.5° (λ ∼ 520 nm) with high quality factors (Q ∼ 260) (Figure 1c). Because these resonances are at the two opposite sides of the Δ point in k space, we denote these modes as W_{TE}-SLR sidebands. The simulated phase map indicates that, at 19°, the incident light travels through the lattice with only minor perturbation by the Ag NPs (Figure 1d). In contrast, at 17.5 and 20.5°, light waves are trapped in the plane of the Ag NP lattice, which results in the strongly modified phase maps. Because the formation of a standing wave with near-zero group velocity in a plasmonic NP lattice is critical to provide optical feedback for lasing,[30,34] the feature of light trapping at 17.5 and 20.5° suggests that these sideband resonances can function as cavity modes for lasing. The hybrid quadrupolar modes excited in the Ag NPs arise from electric field retardation at oblique excitation angles, while the strong electric field enhancement at the surface of the NPs is from the plasmonic character of the W-SLR sidebands (Figure S6).

To determine in more detail how the sidebands of the W_{TE}-SLR mode near the Δ point support lasing, we photoexcited QD-plasmon NP devices using 35 fs, 400 nm laser pulses at

https://dx.doi.org/10.1021/acs.nanolett.9b05342
Nano Lett. 2020, 20, 1468−1474

room temperature and collected the emission spectra at 19° (Figure 2a). At lower pump intensities (<1 mJ/cm^2), the collected emission yielded only a modified photoluminescence (PL) profile (full-width-at-half-maximum (fwhm) ∼5 nm) from the CdSe QD core (Figure 2b). Above a critical pump intensity (>1 mJ/cm^2), a sharp and intense emission peak (λ = 515 nm, fwhm = 1 nm) from the CdS shell appeared close to the wavelength of the sidebands (λ = 520 nm, fwhm = 2 nm) (Figure 1c). Pump energy density versus output intensity curves (plotted on a log−log scale) showed characteristic lasing threshold behavior with a marked change in slope around 1 mJ/cm^2 (Figure 2c). As a control experiment to verify the importance of the plasmonic NP lattices for optical feedback in the hybrid W-SLR mode, we spin-cast a QD film with the same thickness on a fused silica substrate and placed a PDMS slab on top. Without the Ag NP lattice, only amplified spontaneous emission with a larger line width (fwhm ∼20 nm) and lower intensity was observed from the CdS shells (Figure S7). We note that, although the emission wavelength of the CdSe core overlaps with the W-SLR mode at the Γ point (Figure 1b), we did not observe lasing from the core because the small size of the core (3.2 nm in diameter) could not provide enough optical gain to overcome the cavity loss.

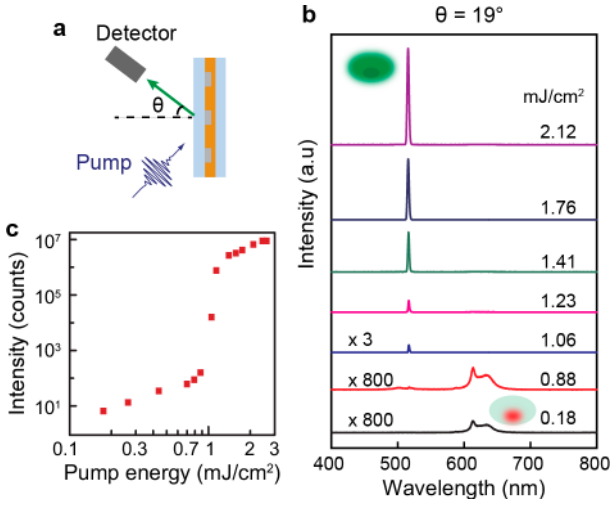

Figure 2. Coherent lasing action from sidebands of the W-SLR mode near the Δ point. (a) Scheme of lasing measurement. (b) Power-dependent spectra at 19°. The inset schemes of QDs represent the core emission at low pump intensity (<1 mJ/cm^2) and the shell emission at high pump intensity (>1 mJ/cm^2). (c) Output emission intensity as a function of input pump pulse energy on a log−log scale.

Figure 3a shows a photograph of the lasing emission, where we placed white paper in front of the QD laser device to capture the four emission beams. Four lasing spots were observed because of the four Δ points along the lattice axis in the $\pm x$ and $\pm y$ directions (Figure 3b). Mapping the pattern of one lasing spot using a camera-based beam profiler revealed a donut-shaped emission with small divergence angle (<2°) (Figure 3c). To investigate the polarization of the lasing mode, we captured the emission pattern at selected polarization directions by inserting a linear polarizer in front of the detector (Figure 3d). At all rotations of the polarizer, the images showed two lobes aligned perpendicular to the polarizer orientation, which indicates that the lasing signals were azimuthally polarized. To determine how the W-SLR sideband modes enable this polarization-dependent lasing, we simulated the optical band structure using the FDTD method. By varying $\mathbf{k}_{\parallel}$ in the θ and ϕ directions near the Δ point, respectively, we found that the W_{TE}-SLR sidebands are excited under s-polarized light along θ and under p-polarized light along ϕ (Figure S8). Because these sideband cavity modes determine the angle and polarization of the amplified photons, lasing exhibits azimuthally polarized beam profiles.

Since the symmetry at the Δ point enables W-SLR sideband modes for off-normal lasing, we further investigated other high-symmetry points in the reciprocal lattice. To achieve emission normal to the surface, we focused on the Γ point in the center of the Brillouin zone. We kept the thickness of the QD film similar to that of the Δ point studies ($t \sim 90$ nm) such that the wavelengths of the W-SLR modes were only determined by the diffraction conditions of the lattice. Reciprocal space analysis shows that four diffraction modes (0, ±1) and (±1, 0) are degenerate at the Γ point ($|\mathbf{k}_{\parallel}| = 0$) (Figure 4a,b). With a_0 = 400 nm, sidebands of the W_{TE}-SLR(1, 0) and W_{TE}-SLR(−1, 0) modes formed near the Γ point ($|\mathbf{k}_{\parallel}| = 0$) around 650 nm (Figure 1b). To exploit the Γ point as optical feedback, we decreased a_0 to 300 nm, which shifted these sidebands to a shorter wavelength range to overlap with the CdS shell emission (Figure 4c and Figure S9). We found that the W-SLR

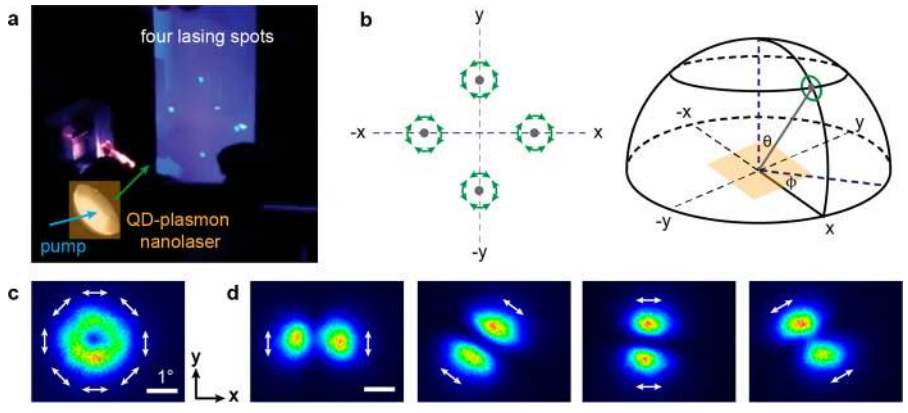

Figure 3. W-SLR sidebands provided optical feedback for four azimuthally polarized lasing beams. (a) Photograph of four lasing spots. (b) Scheme of lasing emission angles and polarization. The green circles show the lasing beams, and the arrows indicate the polarization direction. (c) Far-field emission profile of one lasing spot. White arrows indicate the polarization direction of the output lasing pattern. (d) Beam profiles under selected polarization directions. White arrows show the polarization direction of the linear polarizer in front of the detector.

https://dx.doi.org/10.1021/acs.nanolett.9b05342
Nano Lett. 2020, 20, 1468−1474

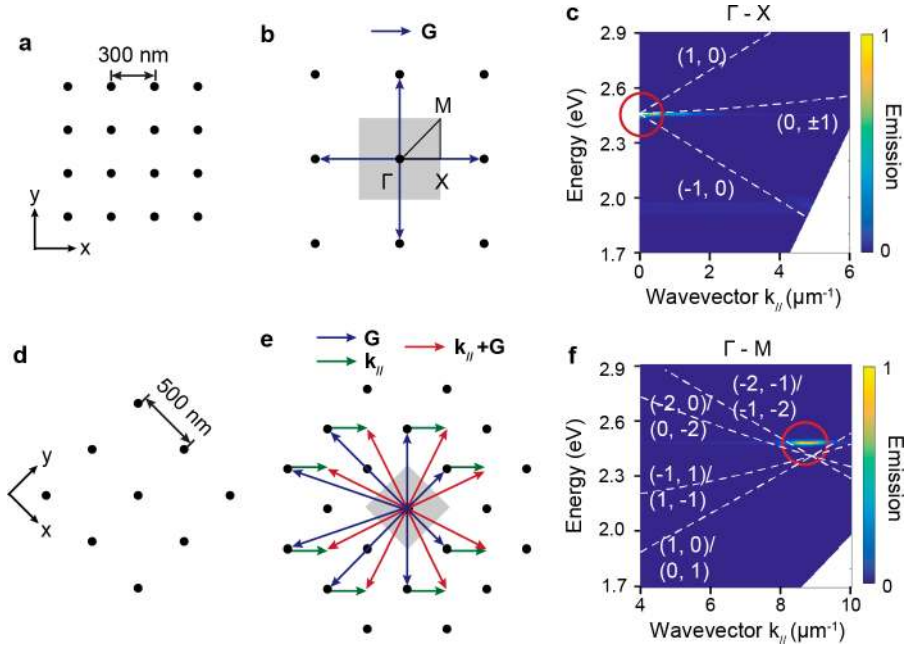

Figure 4. Engineering QD lasing directionality by exploiting other high-symmetry points through different lattice designs. Scheme of the plasmonic lattice with 300 nm periodicity in (a) real space and (b) reciprocal space. The gray area indicates the first Brillouin zone, and the high-symmetry points Γ, X, and M at the boundary of the Brillouin zone. (c) Measured angle-resolved emission showing lasing at the Γ point. White dashed lines are calculated diffraction modes based on the empty-lattice approximation. Scheme of plasmonic lattice with 500 nm periodicity in (d) real space and (e) reciprocal space. Blue arrows indicate the diffraction orders that are degenerate at the M point. Green arrows indicate the direction and magnitude of $\mathbf{k}_{\parallel}$. Red arrows show the direction and magnitude of the net wavevector $\mathbf{k}_{\parallel} + \mathbf{G}$. (f) The measured angle-resolved emission showed lasing at the M point. The thickness of the QD film is ∼90 nm for all panels.

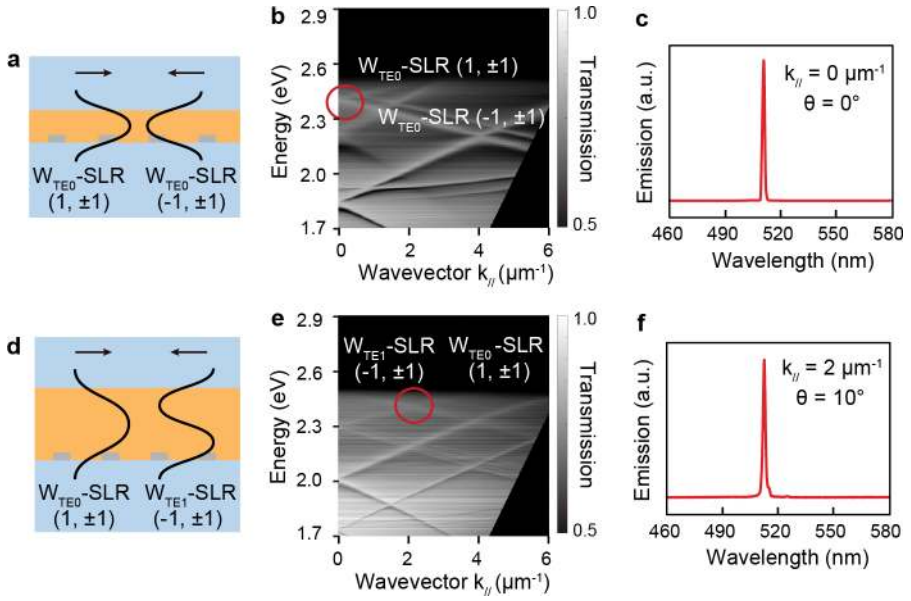

Figure 5. Engineering QD lasing directionality by introducing additional avoided crossings via control over the QD film thickness. (a) Scheme of the QD-plasmon device where the QD film is ∼200 nm thick. (b) Measured band structure under s-polarized incident light along the Γ−X direction. (c) Measured lasing spectrum at 0° normal to the lattice plane. (d) Scheme of the QD-plasmon device where the QD film is ∼350 nm thick. (e) Measured band structure under s-polarized incident light along the Γ−X direction. (f) Measured lasing spectrum at 10°. The periodicity of Ag NP lattices is 400 nm for all panels.

modes near the Γ point support lasing normal to the plane of the NP lattice. The emission profile was stretched along the lattice axes because these W-SLR sidebands (Figure S9) are less dispersive than the sidebands near the Δ point (Figure 1b). We found that the emission pattern has a donut shape, which additionally confirms that the sidebands of the W-SLR modes provide optical feedback (Figure S9).

To expand the range of lasing emission angles, we took advantage of the high-symmetry point M at the boundary of the Brillouin zone for lasing. Because the energies of the diffraction modes are proportional to $|\mathbf{k}_{\parallel} + \mathbf{G}|$, the eight

https://dx.doi.org/10.1021/acs.nanolett.9b05342
Nano Lett. 2020, 20, 1468−1474

diffraction modes (1, 0), (0, 1), (1, −1), (−1, 1), (0, −2), (−2, 0), (−1, −2), and (−2, −1) are degenerate at the M point where $\mathbf{k}_{\parallel} = \frac{1}{2}\mathbf{b_1} + \frac{1}{2}\mathbf{b_2}$ (Figure 4d,e). With a_0 increased to 500 nm, the sidebands of the W-SLR mode near the M point overlap the CdS shell emission, resulting in lasing emission at 45° (Figure 4f and Figure S10). Because of the 4-fold symmetry of the Brillouin zone in the square lattice, lasing showed four emission beams along the diagonal axes of the lattice (Figure S10). We note that the donut-shaped emission profile (Figure S10) was not captured in the angle-resolved emission measurement because of the large collection angle of our detector (∼3°). Also, the slight mismatch between the measured lasing energy and calculated band crossing based on the empty-lattice approximation (Figure 4c,f) is from small variations in effective refractive index because of slight differences in QD film thicknesses.

Although the number of the high-symmetry points in a lattice is limited, tunable laser emission angles can be realized by manipulating the optical band structure through waveguide modes. Since the thickness of the QD film can modulate the effective refractive index of the waveguide mode,[41] the wavelengths of W-SLR modes can be controlled. Similar to the Δ point studies in Figure 1, we kept the periodicity constant (a_0 = 400 nm) and only changed the thickness of the QD film from ∼100 to ∼200 nm to increase the effective refractive index of the waveguide mode (Figure 5a). Under these conditions, sidebands of the W_{TE0}-SLR(1, ±1) and W_{TE0}-SLR(−1, ±1) modes near the Γ point shift to the wavelength range of the QD shell emission (Figure 5b). (Note: Because SLR modes can hybridize with high-order waveguide modes in this structure, we use W_{TE0} to indicate the zeroth-order TE waveguide mode.) As expected, the lasing emission from these cavity modes was normal to the NP lattice plane, and a donut-shaped emission pattern was observed (Figure 5c and Figure S11). Besides tuning the wavelengths of W-SLR modes, a thicker QD film can also enable hybridization of high-order waveguide modes with SLR modes to produce additional avoided crossings in the band structure. We increased the QD film thickness to 350 nm (Figure 5d) while keeping the lattice periodicity unchanged (a_0 = 400 nm), which resulted in the effective refractive index of the first-order TE waveguide mode ($n \sim 1.64$) being lower than the index of the zeroth-order TE waveguide mode ($n \sim 1.87$); the W_{TE1}-SLR (−1, ± 1) modes are higher in energy compared to the W_{TE0}-SLR (−1, ±1) modes. Therefore, the W_{TE1}-SLR (−1, ±1) mode and the W_{TE0}-SLR (1, ±1) mode had an avoided crossing at $|\mathbf{k}_{\parallel}| \sim 2\ \mu m^{-1}$ and not at the Γ point (Figure 5e). The value of $\mathbf{k}_{\parallel}$ for the avoided crossing can be predicted based on the empty-lattice dispersion relations $|\mathbf{k}_{\parallel} + \mathbf{G}_{(1,\pm1)}| = n_{TE0}\frac{\omega}{c}$ and $|\mathbf{k}_{\parallel} + \mathbf{G}_{(-1,\pm1)}| = n_{TE1}\frac{\omega}{c}$. Lasing from these sideband modes showed emission at 10° (Figure 5f and Figure S12).

In summary, we achieved QD shell lasing with engineered beam directionality using plasmonic NP lattices. We demonstrated that overlapping high-symmetry points (Δ, Γ, and M) in the Brillouin zone with the QD gain can facilitate tunable lasing emission at well-defined angles. By increasing the thickness of the QD film, we realized additional avoided crossings in the band structure that now expands the selection of cavity modes for any desired lasing angle. This work provides critical insight into how to manipulate interactions between QDs and optical nanocavities, which is useful for applications in quantum communication and information. Moreover, the engineered band structure in this hybrid waveguide-lattice plasmon system enables opportunities to control strong light−matter interactions for nonlinear optics, photocatalysis, and other optical processes.

■ ASSOCIATED CONTENT

Supporting Information

The Supporting Information is available free of charge at https://pubs.acs.org/doi/10.1021/acs.nanolett.9b05342.

Optical properties of the biaxially strained QDs in solution; optical properties of the closely packed QD thin film; thickness of the QD film; hybridization of waveguide modes and SLR modes; simulated W-SLR sidebands near the Δ point; emission from the QD waveguide without Ag NP lattices; excitation conditions of the W-SLR sidebands near the Δ point; band structure and lasing emission properties near the Γ point; band structure and lasing emission properties near the M point; lasing emission properties from the high-order W-SLR modes (PDF)

■ AUTHOR INFORMATION

Corresponding Author

Teri W. Odom − *Graduate Program in Applied Physics, Department of Materials Science and Engineering, and Department of Chemistry, Northwestern University, Evanston, Illinois 60208, United States;* orcid.org/0000-0002-8490-292X; Email: todom@northwestern.edu

Authors

Jun Guan − *Graduate Program in Applied Physics, Northwestern University, Evanston, Illinois 60208, United States;* orcid.org/0000-0001-8667-1611

Laxmi Kishore Sagar − *Department of Electrical and Computer Engineering, University of Toronto, Toronto M5S 3G4, Canada*

Ran Li − *Department of Materials Science and Engineering, Northwestern University, Evanston, Illinois 60208, United States;* orcid.org/0000-0001-5606-3826

Danqing Wang − *Graduate Program in Applied Physics, Northwestern University, Evanston, Illinois 60208, United States;* orcid.org/0000-0002-7369-1944

Golam Bappi − *Department of Electrical and Computer Engineering, University of Toronto, Toronto M5S 3G4, Canada*

Nicolas E. Watkins − *Department of Chemistry, Northwestern University, Evanston, Illinois 60208, United States*

Marc R. Bourgeois − *Department of Chemistry, Northwestern University, Evanston, Illinois 60208, United States*

Larissa Levina − *Department of Electrical and Computer Engineering, University of Toronto, Toronto M5S 3G4, Canada*

Fengjia Fan − *Department of Electrical and Computer Engineering, University of Toronto, Toronto M5S 3G4, Canada*

Sjoerd Hoogland − *Department of Electrical and Computer Engineering, University of Toronto, Toronto M5S 3G4, Canada*

Oleksandr Voznyy − *Department of Electrical and Computer Engineering, University of Toronto, Toronto M5S 3G4, Canada;* orcid.org/0000-0002-8656-5074

Joao Martins de Pina − *Department of Electrical and Computer Engineering, University of Toronto, Toronto M5S 3G4, Canada*

Richard D. Schaller − *Department of Chemistry, Northwestern University, Evanston, Illinois 60208, United States; Center for Nanoscale Materials, Argonne National Laboratory, Lemont,*

https://dx.doi.org/10.1021/acs.nanolett.9b05342
Nano Lett. 2020, 20, 1468−1474

Illinois 60439, United States; orcid.org/0000-0001-9696-8830

George C. Schatz − *Graduate Program in Applied Physics and Department of Chemistry, Northwestern University, Evanston, Illinois 60208, United States;* orcid.org/0000-0001-5837-4740

Edward H. Sargent − *Department of Electrical and Computer Engineering, University of Toronto, Toronto M5S 3G4, Canada;* orcid.org/0000-0003-0396-6495

Complete contact information is available at: https://pubs.acs.org/10.1021/acs.nanolett.9b05342

Notes

The authors declare no competing financial interest.

■ ACKNOWLEDGMENTS

This work was supported by the National Science Foundation (NSF) under DMR-1904385 and the Vannevar Bush Faculty Fellowship from DOD under N00014-17-1-3023. This work used the Northwestern University Micro/Nano Fabrication Facility (NUFAB), which is partially supported by Soft and Hybrid Nanotechnology Experimental (SHyNE) Resource (NSF ECCS-1542205), the Materials Research Science and Engineering Center (MRSEC) (DMR-1720139), the State of Illinois, and Northwestern University. This work made use of the EPIC, SPID, and Keck-II facilities of Northwestern University's NUANCE Center, which has received support from the SHyNE Resource (NSF ECCS-1542205), the MRSEC program (NSF DMR-1720139) at the Materials Research Center, the International Institute for Nanotechnology (IIN), the Keck Foundation, and the State of Illinois through the IIN. This research was supported in part by the Quest high performance computing facility at Northwestern University, which is jointly supported by the Office of the Provost, the Office for Research, and Northwestern University Information Technology. Use of the Center for Nanoscale Materials, an Office of Science user facility, was supported by the U.S. Department of Energy, Office of Science, Office of Basic Energy Sciences, under Contract No. DE-AC02-06CH11357. This research was supported by the Ontario Research Fund − Research Excellence Program and by the Natural Sciences and Engineering Research Council (NSERC) of Canada.

■ REFERENCES

(1) Wang, Y.; Sun, H. D. Advances and Prospects of Lasers Developed from Colloidal Semiconductor Nanostructures. *Prog. Quantum Electron.* **2018**, *60*, 1−29.

(2) Talapin, D. V.; Lee, J. S.; Kovalenko, M. V.; Shevchenko, E. V. Prospects of Colloidal Nanocrystals for Electronic and Optoelectronic Applications. *Chem. Rev.* **2010**, *110*, 389−458.

(3) Yin, Y.; Alivisatos, A. P. Colloidal Nanocrystal Synthesis and the Organic-Inorganic Interface. *Nature* **2005**, *437*, 664−670.

(4) Chen, O.; Zhao, J.; Chauhan, V. P.; Cui, J.; Wong, C.; Harris, D. K.; Wei, H.; Han, H. S.; Fukumura, D.; Jain, R. K.; Bawendi, M. G. Compact High-Quality Cdse-Cds Core-Shell Nanocrystals with Narrow Emission Linewidths and Suppressed Blinking. *Nat. Mater.* **2013**, *12*, 445−451.

(5) Nurmikko, A. What Future for Quantum Dot-Based Light Emitters? *Nat. Nanotechnol.* **2015**, *10*, 1001−1004.

(6) Klimov, V. I.; Mikhailovsky, A. A.; Xu, S.; Malko, A.; Hollingsworth, J. A.; Leatherdale, C. A.; Eisler, H. J.; Bawendi, M. G. Optical Gain and Stimulated Emission in Nanocrystal Quantum Dots. *Science* **2000**, *290*, 314−317.

(7) Pietryga, J. M.; Park, Y. S.; Lim, J. H.; Fidler, A. F.; Bae, W. K.; Brovelli, S.; Klimov, V. I. Spectroscopic and Device Aspects of Nanocrystal Quantum Dots. *Chem. Rev.* **2016**, *116*, 10513−10622.

(8) le Feber, B.; Prins, F.; De Leo, E.; Rabouw, F. T.; Norris, D. J. Colloidal-Quantum-Dot Ring Lasers with Active Color Control. *Nano Lett.* **2018**, *18*, 1028−1034.

(9) Krahne, R.; Zavelani-Rossi, M.; Lupo, M. G.; Manna, L.; Lanzani, G. Amplified Spontaneous Emission from Core and Shell Transitions in Cdse/Cds Nanorods Fabricated by Seeded Growth. *Appl. Phys. Lett.* **2011**, *98*, 063105.

(10) Garcia-Santamaria, F.; Chen, Y. F.; Vela, J.; Schaller, R. D.; Hollingsworth, J. A.; Klimov, V. I. Suppressed Auger Recombination in "Giant" Nanocrystals Boosts Optical Gain Performance. *Nano Lett.* **2009**, *9*, 3482−3488.

(11) Snee, P. T.; Chan, Y. H.; Nocera, D. G.; Bawendi, M. G. Whispering-Gallery-Mode Lasing from a Semiconductor Nanocrystal/Microsphere Resonator Composite. *Adv. Mater.* **2005**, *17*, 1131−1136.

(12) Grivas, C.; Li, C. Y.; Andreakou, P.; Wang, P. F.; Ding, M.; Brambilla, G.; Manna, L.; Lagoudakis, P. Single-Mode Tunable Laser Emission in the Single-Exciton Regime from Colloidal Nanocrystals. *Nat. Commun.* **2013**, *4*, 2376.

(13) Roh, K.; Dang, C.; Lee, J.; Chen, S. T.; Steckel, J. S.; Coe-Sullivan, S.; Nurmikko, A. Surface-Emitting Red, Green, and Blue Colloidal Quantum Dot Distributed Feedback Lasers. *Opt. Express* **2014**, *22*, 18800−18806.

(14) Dang, C.; Lee, J.; Breen, C.; Steckel, J. S.; Coe-Sullivan, S.; Nurmikko, A. Red, Green and Blue Lasing Enabled by Single-Exciton Gain in Colloidal Quantum Dot Films. *Nat. Nanotechnol.* **2012**, *7*, 335−339.

(15) Kress, S. J. P.; Cui, J.; Rohner, P.; Kim, D. K.; Antolinez, F. V.; Zaininger, K. A.; Jayanti, S. V.; Richner, P.; McPeak, K. M.; Poulikakos, D.; Norris, D. J. A Customizable Class of Colloidal-Quantum-Dot Spasers and Plasmonic Amplifiers. *Sci. Adv.* **2017**, *3*, e1700688.

(16) Niven, G.; Mooradian, A. Trends in Laser Light Sources for Projection Display. *Idw '06: Proceedings of the 13th International Display Workshops*, Vols. *1*−*3*; 2006; pp 1939−1942.

(17) Fujii, T.; Fukuchi, T. *Laser Remote Sensing*; CRC Press: 2005.

(18) Borkar, S. Role of Interconnects in the Future of Computing. *J. Lightwave Technol.* **2013**, *31*, 3927−3933.

(19) Haurylau, M.; Chen, H.; Zhang, J. D.; Chen, G. Q.; Nelson, N. A.; Albonesi, D. H.; Friedman, E. G.; Fauchet, P. M. On-Chip Optical Interconnect Roadmap: Challenges and Critical Directions. *2005 2nd IEEE International Conference on Group IV Photonics* **2005**, 17−19.

(20) Zou, S. L.; Janel, N.; Schatz, G. C. Silver Nanoparticle Array Structures That Produce Remarkably Narrow Plasmon Lineshapes. *J. Chem. Phys.* **2004**, *120*, 10871−10875.

(21) Auguie, B.; Barnes, W. L. Collective Resonances in Gold Nanoparticle Arrays. *Phys. Rev. Lett.* **2008**, *101*, 143902.

(22) Yang, A. K.; Hoang, T. B.; Dridi, M.; Deeb, C.; Mikkelsen, M. H.; Schatz, G. C.; Odom, T. W. Real-Time Tunable Lasing from Plasmonic Nanocavity Arrays. *Nat. Commun.* **2015**, *6*, 6939.

(23) Wang, D. Q.; Yang, A. K.; Hryn, A. J.; Schatz, G. C.; Odom, T. W. Superlattice Plasmons in Hierarchical Au Nanoparticle Arrays. *ACS Photonics* **2015**, *2*, 1789−1794.

(24) Knudson, M. P.; Li, R.; Wang, D. Q.; Wang, W. J.; Schaller, R. D.; Odom, T. W. Polarization-Dependent Lasing Behavior from Low-Symmetry Nanocavity Arrays. *ACS Nano* **2019**, *13*, 7435−7441.

(25) Li, R.; Bourgeois, M. R.; Cherqui, C.; Guan, J.; Wang, D. Q.; Hu, J. T.; Schaller, R. D.; Schatz, G. C.; Odom, T. W. Hierarchical Hybridization in Plasmonic Honeycomb Lattices. *Nano Lett.* **2019**, *19*, 6435−6441.

(26) Zhou, W.; Odom, T. W. Tunable Subradiant Lattice Plasmons by out-of-Plane Dipolar Interactions. *Nat. Nanotechnol.* **2011**, *6*, 423−427.

(27) Yang, A.; Hryn, A. J.; Bourgeois, M. R.; Lee, W.-K.; Hu, J.; Schatz, G. C.; Odom, T. W. Programmable and Reversible Plasmon

Mode Engineering. *Proc. Natl. Acad. Sci. U. S. A.* **2016**, *113*, 14201−14206.
(28) Lin, Y. H.; Wang, D. Q.; Hu, J. T.; Liu, J. X.; Wang, W. J.; Guan, J.; Schaller, R. D.; Odom, T. W. Engineering Symmetry-Breaking Nanocrescent Arrays for Nanolasing. *Adv. Funct. Mater.* **2019**, *29*, 1904157.
(29) Wang, D.; Bourgeois, M. R.; Lee, W. K.; Li, R.; Trivedi, D.; Knudson, M. P.; Wang, W.; Schatz, G. C.; Odom, T. W. Stretchable Nanolasing from Hybrid Quadrupole Plasmons. *Nano Lett.* **2018**, *18*, 4549−4555.
(30) Zhou, W.; Dridi, M.; Suh, J. Y.; Kim, C. H.; Co, D. T.; Wasielewski, M. R.; Schatz, G. C.; Odom, T. W. Lasing Action in Strongly Coupled Plasmonic Nanocavity Arrays. *Nat. Nanotechnol.* **2013**, *8*, 506−511.
(31) Wang, W. J.; Watkins, N.; Yang, A. K.; Schaller, R. D.; Schatz, G. C.; Odom, T. W. Ultrafast Dynamics of Lattice Plasmon Lasers. *J. Phys. Chem. Lett.* **2019**, *10*, 3301−3306.
(32) Fernandez-Bravo, A.; Wang, D. Q.; Barnard, E. S.; Teitelboim, A.; Tajon, C.; Guan, J.; Schatz, G. C.; Cohen, B. E.; Chan, E. M.; Schuck, P. J.; Odom, T. W. Ultralow-Threshold, Continuous-Wave Upconverting Lasing from Subwavelength Plasmons. *Nat. Mater.* **2019**, *18*, 1172−1176.
(33) Wang, D. Q.; Guan, J.; Hu, J. T.; Bourgeois, M. R.; Odom, T. W. Manipulating Light-Matter Interactions in Plasmonic Nanoparticle Lattices. *Acc. Chem. Res.* **2019**, *52*, 2997−3007.
(34) Wang, D.; Yang, A.; Wang, W.; Hua, Y.; Schaller, R. D.; Schatz, G. C.; Odom, T. W. Band-Edge Engineering for Controlled Multi-Modal Nanolasing in Plasmonic Superlattices. *Nat. Nanotechnol.* **2017**, *12*, 889−894.
(35) Hakala, T. K.; Rekola, H. T.; Vakevainen, A. I.; Martikainen, J. P.; Necada, M.; Moilanen, A. J.; Torma, P. Lasing in Dark and Bright Modes of a Finite-Sized Plasmonic Lattice. *Nat. Commun.* **2017**, *8*, 13687.
(36) Guo, R.; Necada, M.; Hakala, T. K.; Vakevainen, A. I.; Torma, P. Lasing at K Points of a Honeycomb Plasmonic Lattice. *Phys. Rev. Lett.* **2019**, *122*, 013901.
(37) Lee, M. H.; Huntington, M. D.; Zhou, W.; Yang, J.-c.; Odom, T. W. Programmable Soft Lithography: Solvent-Assisted Nanoscale Embossing. *Nano Lett.* **2011**, *11*, 311−315.
(38) Henzie, J.; Kwak, E. S.; Odom, T. W. Mesoscale Metallic Pyramids with Nanoscale Tips. *Nano Lett.* **2005**, *5*, 1199−1202.
(39) Gao, H.; Henzie, J.; Odom, T. W. Direct Evidence for Surface Plasmon-Mediated Enhanced Light Transmission through Metallic Nanohole Arrays. *Nano Lett.* **2006**, *6*, 2104−2108.
(40) Fan, F. J.; Voznyy, O.; Sabatini, R. P.; Bicanic, K. T.; Adachi, M. M.; McBride, J. R.; Reid, K. R.; Park, Y. S.; Li, X. Y.; Jain, A.; Quintero-Bermudez, R.; Saravanapavanantham, M.; Liu, M.; Korkusinski, M.; Hawrylak, P.; Klimov, V. I.; Rosenthal, S. J.; Hoogland, S.; Sargent, E. H. Continuous-Wave Lasing in Colloidal Quantum Dot Solids Enabled by Facet-Selective Epitaxy. *Nature* **2017**, *544*, 75−79.
(41) Adams, M. J. *An Introduction to Optical Waveguides*; John Wiley & Sons: New York, 1981.

https://dx.doi.org/10.1021/acs.nanolett.9b05342
Nano Lett. 2020, 20, 1468−1474